



HAL
open science

Recent trends in hydrogen and oxygen electrocatalysis for anion exchange membrane technologies

Aurélien Habrioux, Claudia Morais, Teko Napporn, Boniface Kokoh

► To cite this version:

Aurélien Habrioux, Claudia Morais, Teko Napporn, Boniface Kokoh. Recent trends in hydrogen and oxygen electrocatalysis for anion exchange membrane technologies. *Current Opinion in Electrochemistry*, 2020, 21, pp.146-159. 10.1016/j.coelec.2020.01.018 . hal-03049262

HAL Id: hal-03049262

<https://hal.science/hal-03049262>

Submitted on 9 Dec 2020

HAL is a multi-disciplinary open access archive for the deposit and dissemination of scientific research documents, whether they are published or not. The documents may come from teaching and research institutions in France or abroad, or from public or private research centers.

L'archive ouverte pluridisciplinaire **HAL**, est destinée au dépôt et à la diffusion de documents scientifiques de niveau recherche, publiés ou non, émanant des établissements d'enseignement et de recherche français ou étrangers, des laboratoires publics ou privés.

Recent trends in hydrogen and oxygen electrocatalysis for anion exchange membrane technologies

Aurélien Habrioux*, Claudia Morais, Teko W. Napporn, Boniface Kokoh*

Université de Poitiers, Institut de Chimie des Milieux et Matériaux de Poitiers (IC2MP),
UMR-CNRS 7285, 4, Rue Michel Brunet, TSA 51106, F-86073 Poitiers, France

Keywords: Hydrogen evolution reaction, hydrogen oxidation reaction, oxygen reduction reaction, oxygen evolution reaction, electrocatalysis, alkaline electrolytes

Abstract

This review aims at presenting recent findings in the understanding of oxygen and hydrogen electrocatalysis in alkaline electrolytes that are key processes for the emergence of sustainable energy storage and conversion devices such as anion exchanged membrane fuel cells and electrolyzers. In these systems, the exchange of electrons through electrochemical reactions provides a unique pathway to reversibly convert the electricity vector into chemical one: hydrogen. A concise and critical review of advances made during the last past years in the design of catalysts is provided. Challenges and opportunities for the development of the next catalyst generation are also addressed.

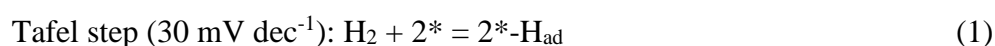
1. Introduction

Storing and then using renewable resources are sustainable processes to reduce fossil fuel consumption. The production of clean hydrogen in a water electrolyzer and its further combustion in a fuel cell to deliver heat, electricity and only water as by-product are thereby sustainable perspectives [1] for the implementation of a future energy grid based on a hydrogen economy. Hydrogen as well as oxygen electrocatalysis will govern electrical performances of the above-mentioned applications. The recent development of anion exchange membranes [2] with useful conductivities in the range of 20-40 mS cm⁻¹ [3] paved the way for the design of solid anion exchange membrane technologies, recently reinforcing the interest to design catalysts evolving in alkaline environments. These media allow using catalysts free from PGM and even free from critical raw materials [4]. In this review, recent advances in the design of catalysts and in the understanding of their activity towards key hydrogen evolution (HER), hydrogen oxidation (HOR), oxygen evolution (OER) and oxygen reduction (ORR) reactions in alkaline medium are discussed. In this review, the emphasis will be mainly on recent developments made in the design of non-PGM based catalysts.

2. Hydrogen electrocatalysis in alkaline medium

2.1 Understanding factors affecting hydrogen electrocatalysis in alkaline medium

Hydrogen electrocatalysis has been extensively studied to lay the basis of modern electrocatalysis [5]. Reaction mechanisms generally imply three different elementary steps (Heyrovsky-Volmer or Tafel-Volmer mechanisms) that can be described as follows in alkaline electrolytes (* refers to a catalytic site):





To be more informative, HER/HOR mechanisms have been illustrated in Figure 1.

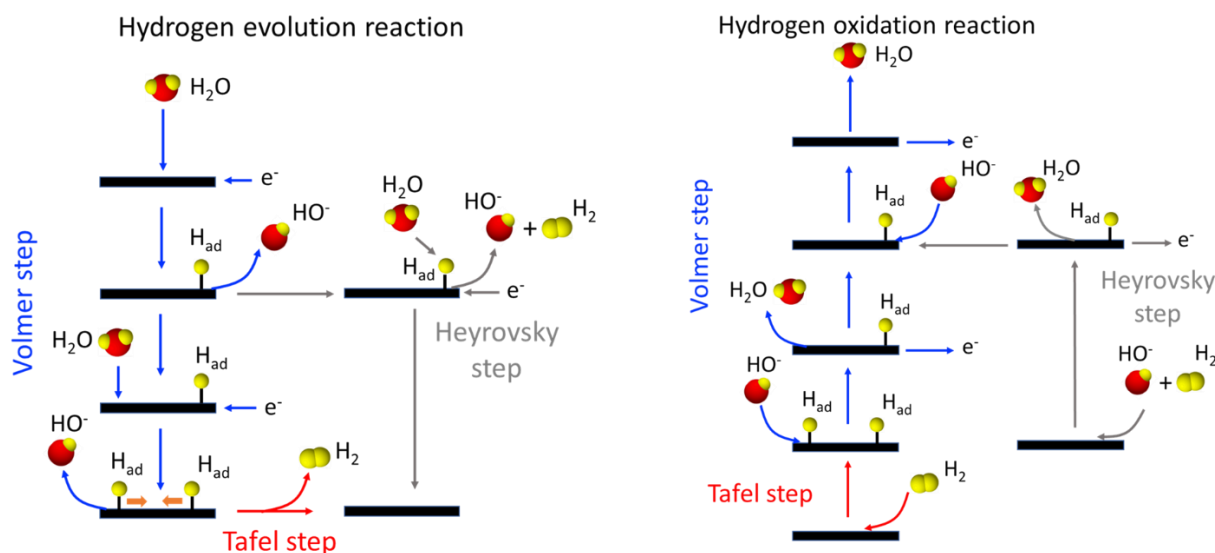


Figure 1: Illustration of HER and HOR mechanisms in alkaline medium

HOR/HER have been largely investigated in acidic electrolytes [6] and reactivity of PGM-based catalysts was shown to be lower by at least two orders of magnitude in alkaline media [7, 8] making it difficult to explain reactivity with a simple descriptor. It was first proposed that metal-hydrogen bond strength increased with pH value in agreement with the position of Hupd peaks [9]. Nevertheless, this quite simple correlation has to be reviewed since Hupd peaks position depends both on Pt surface oxophilicity [10] and the adsorption of cations from the alkaline electrolyte [11]. Recently, Strmcnik et al. [12, 13], showed that three main factors affect HOR and HER kinetics. In addition to H adsorption energy, the nature of the proton source (oxonium ion in acidic medium or water in alkaline medium) as well as the presence of surface species (hydroxides, electrolyte ions) should be considered to explain HOR/HER activity of a material. The two latter phenomena are responsible for modifying both adsorption energy of hydrogen and water molecules, thus particularly affecting kinetics of the Volmer step (3). Furthermore, very recently, the role played by the formation of $\text{OH}_{\text{ad}}\text{-(H}_2\text{O)}_{\text{x}}$ -

AM^+ (with AM^+ = alkali metal cation) adducts in alkaline electrolytes has been brought to light and has been shown to be responsible for destabilizing OH_{ad} , thus limiting the rate of HOR whereas promoting HER kinetics [14]. From the previous discussion, it appears that tuning of OH adsorption energy at a catalyst surface is a promising pathway to improve its catalytic efficiency towards hydrogen electrocatalysis.

2.2 Catalysts for HOR/HER in alkaline medium

PGM-based catalysts (based on the use of Pd, Pt, Ir, Ru) are the most efficient ones towards HOR in alkaline medium. Numerous strategies (substrate engineering, alloying effect, particle size effect) have been employed to improve their activity and recently reviewed [15]. During the last years, research efforts were focused on the alloying of noble metals (Pt or Pd) with oxophilic atoms such as Ru and Ni [13, 16, 17]. As an example, resulting Pt/Ru catalyst exhibited a very high HOR activity (see Table 1) in reason of the promotion of OH adsorption. The same kind of effects was observed by depositing Pd nanocrystals onto oxophilic ceria [18]. Non-noble metal-based catalysts presenting a significant HOR activity are exclusively based on the use of Ni. Performances of such catalysts are presented in Table 1. Alloying Ni with Co and Mo allowed obtaining a very active CoNiMo catalyst [19] presenting a hydrogen binding energy close to that of Pt. The synthesis and the use of N-doped carbon nanotubes supported Ni nanoparticles as catalyst allowed achieving a very high HOR kinetics [20], in reason of the electronic modulation of Ni resulting from the interaction between Ni and N-edge atoms grafted onto the carbon substrate. The substrate engineering appears then as a reliable strategy to modulate hydrogen bonding energy at a catalytic surface. More recently, a Ni_3N/C catalyst was synthesized and exhibited a huge activity towards HOR in reason of a downshift of the Ni d-band weakening binding energy of hydrogen as well as oxygenated species [21]. As reviewed in 2015 [1], HER catalysts can be classified into three main subclasses comprising PGM-based catalysts [22], transition-metal carbides [23], oxides

[24], sulfides [25], selenides [26], phosphides [27], nitrides [28], borides [29] and non-metal catalysts based on the use of C, N, S elements [30]. In 2011, Markovic et al. reported a heterostructured catalyst composed of Pt decorated with Ni(OH)₂ clusters. This material exhibited an enhanced HER activity in comparison with the Pt platinum pristine surface. The presence of Ni(OH)₂ favored water dissociation and then faster kinetics for the Volmer step [31]. Based on the same concept a Pt/Ni(HCO₃)₂ catalyst was very recently designed and exhibited a huge HER activity with an overpotential as low as 27 mV to achieve a current density of -10 mA cm⁻² [22]. Recently, numerous nanostructured non-noble metal-based with heterojunctions were developed, some of them being more active than Pt/C catalysts in reason of the lowering of adsorption free energy of H at heterointerfaces [32]. These heterostructured catalysts often combine at least two different efficient catalysts towards HER [25]. This concept was then used to perform the growth of heterostructured catalysts composed of sulfides [33] or phosphides [34] directly onto Ni foam. The established interfaces allow facilitating both chemisorption of hydrogen and oxygen intermediates, thus improving the overall water splitting activity [33]. Another recent trend consists in atomically engineering active sites by doping a poorly active HER catalyst. This allows tuning electron density of active sites, thus modifying H adsorption energy and favoring the cleavage of water molecule [35-37]. HER/HOR activities of previously described materials are reported in Table 1.

Table 1: Non-exhaustive list presenting representative recently developed catalysts for HER/HOR in alkaline medium. j_0 represents the exchange current density. It has been normalized using either platinum active surface area (in that case the unit is denoted as mg cm⁻²_{Pt}) or using geometric surface area. The mass normalized j_0 value is also given for HOR catalysts. η represents the overpotential. For HER, overpotential values at -10 mA cm⁻² (η_{-10}) as well as at -100 mA cm⁻² (η_{-100}) are given. b is the Tafel slope.

Hydrogen oxidation reaction (HOR)	Catalyst	Morphology / structure	Loading ($\text{mg}_{\text{metal}} \text{cm}^{-2}$)	Working electrode	Electrolyte	j_0 ($\text{mA mg}^{-1}_{\text{metal}}$)	j_0 ($\text{mA cm}^{-2}_{\text{metal}}$)	Activity at $\eta = 50 \text{ mV}$	Ref.	
	Pt	Nanowires	0.02	Vulcan XC 72 R coated glassy carbon	0.1 M KOH	$16 \text{ mA mg}^{-1}_{\text{Pt}}$	$0.229 \text{ mA cm}^{-2}_{\text{Pt}}$	$69 \text{ mA mg}^{-1}_{\text{Pt}}$	[17]	
	PtRu	Nanowires	0.02	Vulcan XC 72 R coated glassy carbon	0.1 M KOH	$32 \text{ mA mg}^{-1}_{\text{Pt}}$	$0.493 \text{ mA cm}^{-2}_{\text{Pt}}$	$160 \text{ mA mg}^{-1}_{\text{Pt}}$		
	PtFe	Nanowires	0.02	Vulcan XC 72 R coated glassy carbon	0.1 M KOH	$27 \text{ mA mg}^{-1}_{\text{Pt}}$	$0.459 \text{ mA cm}^{-2}_{\text{Pt}}$	$122 \text{ mA mg}^{-1}_{\text{Pt}}$		
	CoMoNi	Electroplated material	n/a	Au	0.1 M KOH	n/a	0.015	$0.044 \text{ mA cm}^{-2}_{\text{metal}}$	[19]	
	Pt	polycrystalline disk	n/a	Pt	0.1 M KOH	n/a	0.61	$1.4 \text{ mA cm}^{-2}_{\text{metal}}$		
	Ni/N-CNT	Nanoparticles (20 nm)	0.25	Glassy carbon	0.1 M KOH	3.5	0.028	$9.3 \text{ mA mg}^{-1}_{\text{metal}}$	[20]	
	Ni ₃ N/C	Nanoparticles (4.6 nm)	0.16	Glassy carbon	0.1 M KOH	12	0.014	$24.4 \text{ mA mg}^{-1}_{\text{metal}}$	[21]	
Hydrogen evolution reaction (HER)	Catalyst	Morphology / structure	Loading (mg cm^{-2})	Working electrode	Electrolyte	η_{-10} (mV)	η_{-100} (mV)	j_0 (mA cm^{-2})	b (mV dec^{-1})	Ref.
	Pt/Ni(HCO ₃) ₂	20 wt. % Pt nanoparticles (2-3 nm) on Ni(HCO ₃) ₂ nanoplates	0.04	Glassy carbon	1 M KOH	-27	ca. -70 mV	$5.6 \text{ mA cm}^{-2}_{\text{Pt}}$	40	[22]
	Pt	Bare Pt nanoparticles	0.2	Glassy carbon	1 M KOH	-44	ca. -125 mV	$2.8 \text{ mA cm}^{-2}_{\text{Pt}}$	52	
	Pt/C	Commercial 10 wt.% Pt/C (Sigma-Aldrich)	0.02	Glassy carbon	1 M KOH	ca. -50	n/a	n/a	104	
	Mo ₂ C/N-doped carbon microflowers	N-doped microflowers consisting of nanoflakes decorated with β -Mo ₂ C (particles)	0.28	Glassy carbon	1 M KOH	-100	n/a	n/a	65	[23]
	Pt/C	Commercial 20 wt. % Pt/C	0.28	Glassy carbon	1 M KOH	-50	n/a	n/a	34	
	Fe _{1.89} Mo _{4.11} O ₇	Microparticles	2.4	Bare carbon paste	1 M KOH	-197	n/a	0.069	79	[24]
	Pt/C	Commercial 20 wt. % Pt/C	n/a	n/a	1 M KOH	-103	n/a	n/a	27	
	NiS ₂ /MoS ₂	Hybrid porous nanowires composed of MoS ₂ nanoplates and NiS ₂ particles with heterojunctions	0.2	Glassy carbon	1 M KOH	-204	n/a	n/a	65	[25]
	Pt/C	n/a	0.2	Glassy carbon	1 M KOH	-50	n/a	n/a	35	
	FeNiSe/exfoliated graphene	Mesoporous FeNiSe nanosheets grown onto exfoliated graphene	3.3	Graphite foil	1 M KOH	-187	n/a	0.57	65	[26]
	Pt/C	Commercial catalyst	3.3	n/a	1 M KOH	ca.-75	n/a	n/a	46	

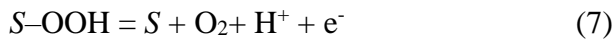
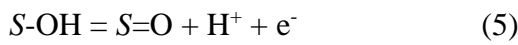
Mn-doped Ni ₂ P	Mn-doped Ni ₂ P Nanosheets array on Ni foam	n/a	Ni foam	1 M KOH	ca. 50	ca. -220	n/a	135	[27]
Pt/C	Commercial 20 wt. % Pt/C (Sigma-Aldrich)	7.0	Ni foam	1 M KOH	ca. 20	ca. -120	n/a	98	
NiCoN/C	Hybrid nanocages composed of nanosheets with a thickness of 2-3 nm	0.2	Glassy carbon	1 M KOH	-103	n/a	n/a	n/a	[28]
Pt/C	Commercial Pt/C	0.05	Glassy carbon	1 M KOH	-91	n/a	n/a	n/a	
Co-Ni-B/carbon cloth	Co-Ni-B nanoparticles (5-10 nm)	0.34	Carbon cloth	1 M KOH	-80	ca. -250	n/a	88	[29]
Pt/C	Commercial Pt/C	0.34	Carbon cloth	1 M KOH	ca. -25	ca. -240	n/a	30	
S-doped C ₃ N ₄ /carbon naotubes/carbon fiber	Fibers decorated with S-doped C ₃ N ₄	0.5	Carbon fiber	1 M KOH	-131	ca. -250	0.28	79	[30]
Mo ₂ C/Mo ₂ N	Mesoporous material	0.38	Glassy carbon	1 M KOH	-145	-222	0.05	55	[32]
Pt/C	20 wt. % Pt/C (Alfa Aesar)	0.38	Glassy carbon	1 M KOH	-60	-263	5.87 mA cm ⁻² _{Pt}	47	
MoS ₂ /Ni ₃ S ₂ /nickel foam	Porous heterostructure grown onto Ni foam	9.7	Ni foam	1 M KOH	ca. -110	n/a	n/a	83	[33]
Pt/C	20 wt. % Pt/C (Fuel Cell store)	0.8	Ni foam	1 M KOH	ca. -25	n/a	n/a	32	
FeP/Ni ₂ P/nickel foam	Porous heterostructures composed of FeP and Ni ₂ P nanoparticles grown onto Ni foam	8	Ni foam	1 M KOH	-14	ca. -130	n/a	24	[34]
Pt	Pt wire	n/a	n/a	1 M KOH	-59	ca. -130	n/a	37	
N-NiCo ₂ S ₄	Nanowires	n/a	Ni foam	1 M KOH	-41	ca. -140	n/a	37	[36]
Pt/C	Commercial 20 wt. % Pt/C	2.3	Ni foam	1 M KOH	-28	ca. -140	n/a	29	
Ni, Zn-doped CoO	Nanorods	0.486	Carbon fiber paper	1 M KOH	-53	ca. -160	n/a	47	[37]
Pt/C	Commercial 20 wt. % Pt/C (Fuel cell store)	0.4	Carbon fiber paper	1 M KOH	ca. -60	ca. -175	n/a	33	

	NiO@1T-MoS ₂ /CFP	Nanosheets	1.02	Carbon fiber paper	1 M KOH	-46	ca. -120	0.44	52	[35]
	Pt/C	Commercial 20 wt. % Pt/C (Johnson Matthey)	1	Carbon fiber paper	1 M KOH	-23	ca. -130	0.69	32	

3. Oxygen electrocatalysis in alkaline medium

3.1 Origin of oxygen electrode overpotentials

OER/ORR kinetic limitations can be described assuming a reaction mechanism composed of four proton coupled electron transfer steps and implying three reaction intermediates ($S=O$, $S-OH$ and $S-OOH$, where S denotes a catalytic site). This reaction mechanism can be described using the following equations (4)-(7):



From these reactions, the different reaction energies can be expressed as follows taking water as the origin of the energy scale:

$$\Delta G_1 = \Delta G_{OH} - \Delta G_{H_2O} = \Delta G_{OH} \quad (8)$$

$$\Delta G_2 = \Delta G_O - \Delta G_{OH} \quad (9)$$

$$\Delta G_3 = \Delta G_{OOH} - \Delta G_O \quad (10)$$

$$\Delta G_4 = \Delta G_{O_2} - \Delta G_{OOH} = 4.92 - \Delta G_{OOH} \quad (11)$$

Considering that total energy required to transform H_2O into O_2 is 4.92 eV (4×1.23 eV) as well as that $S-OH$ and $S=O$ are respectively singly and doubly bonded reaction intermediates, equations (8)-(11) can be written, as follows [38]:

$$\Delta G_1 = \Delta G_2 \quad (12)$$

$$\sum_{i=1 \text{ to } 4} \Delta G_i = 4.92 \text{ eV} \quad (13)$$

$$\Delta G_4 = 4.92 - \Delta G_3 - 2\Delta G_1 \quad (14)$$

Thus ΔG_i can be described using two independent parameters, that is to know ΔG_1 and ΔG_3 . The overpotential required for OER/ORR is obviously governed by the step with highest energy barrier.

Thus, ORR/OER overpotentials can be described with the following equations [38, 39]:

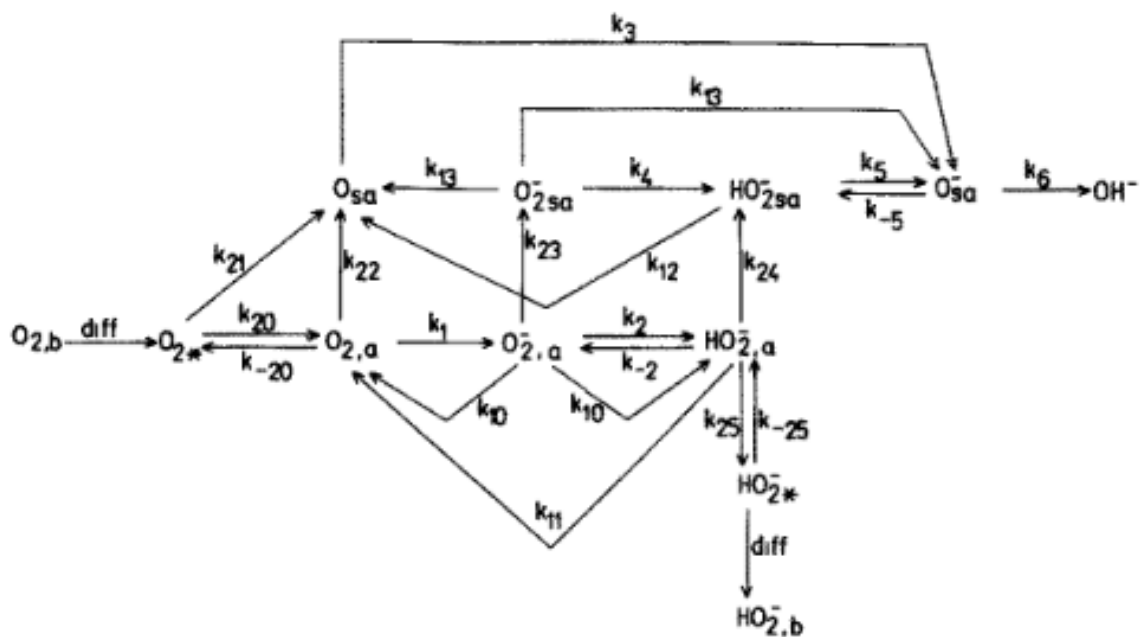
$$\eta_{OER} = \frac{\text{Max}(\Delta G_i)_{i=1 \text{ to } 4}}{e} - 1.23 \quad (15)$$

$$\eta_{ORR} = \frac{\text{Min}(\Delta G_i)_{i=1 \text{ to } 4}}{e} - 1.23 \quad (16)$$

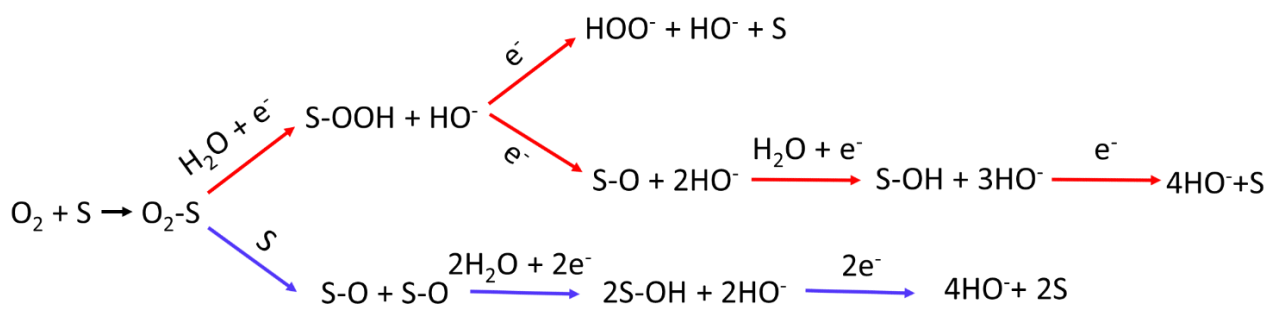
where e is the elementary charge.

For an ideal catalyst, it is observed that $(\Delta G_i)_{i=1 \text{ to } 4} = \frac{4.92}{4} = 1.23 \text{ eV}$ meaning that ΔG_{OH} , ΔG_O and ΔG_{OOH} are respectively equal to 1.23, 2.46 and 3.69 eV [40]. In such case, the energy difference $\Delta G_{OOH} - \Delta G_{OH}$ is equal to 2.46 eV. The transition from one intermediate to another is thus spontaneous for an electrode potential of 1.23 V vs. RHE. To optimize a real catalyst, it is required to reach a situation where $\Delta G_1 = \Delta G_3 = 1.23 \text{ eV}$. For this purpose, ΔG_{OH} and ΔG_{OOH} have to be tuned independently [38]. Nevertheless, as oxygenated intermediates are chemically bonded to the catalyst surface through O atom, binding energies of S-OH and S-OOH are interdependent [40, 41] and linearly scaled, rendering impossible their separate optimization. Furthermore, the energy difference $\Delta G_{OOH} - \Delta G_{OH}$ is nearly constant whatever the considered materials and is equal to 3.2 eV [39], far from the ideal value of 2.46 eV. For the real catalyst, at 1.23 V vs. RHE, all steps are not downhill processes. Applying an electrode potential away from 1.23 V vs. RHE is thus required. Comparison between different catalysts families using this theoretical framework is nevertheless only possible if catalytic surfaces follow the same reaction mechanism. That is not the case for all catalysts families and OER/ORR mechanisms are still under debate. Some recent studies pointed out that breaking scaling relations are a required but not sufficient condition to optimize the activity of a catalyst and the potential determining step has to be considered through the examination and comparison of the electrochemical-step symmetry index value with overpotential [39, 42].

Furthermore, recent progress made to better include solvent effects (likely causing stabilization of intermediates) in models enabled greatly to improve the accuracy of theoretical results to describe OER/ORR kinetics [43] at catalyst surfaces. Some of the proposed ORR/OER mechanisms for various electrocatalysts in alkaline medium are presented in Figure 2 on the basis of several references [44-48].



a)



b)

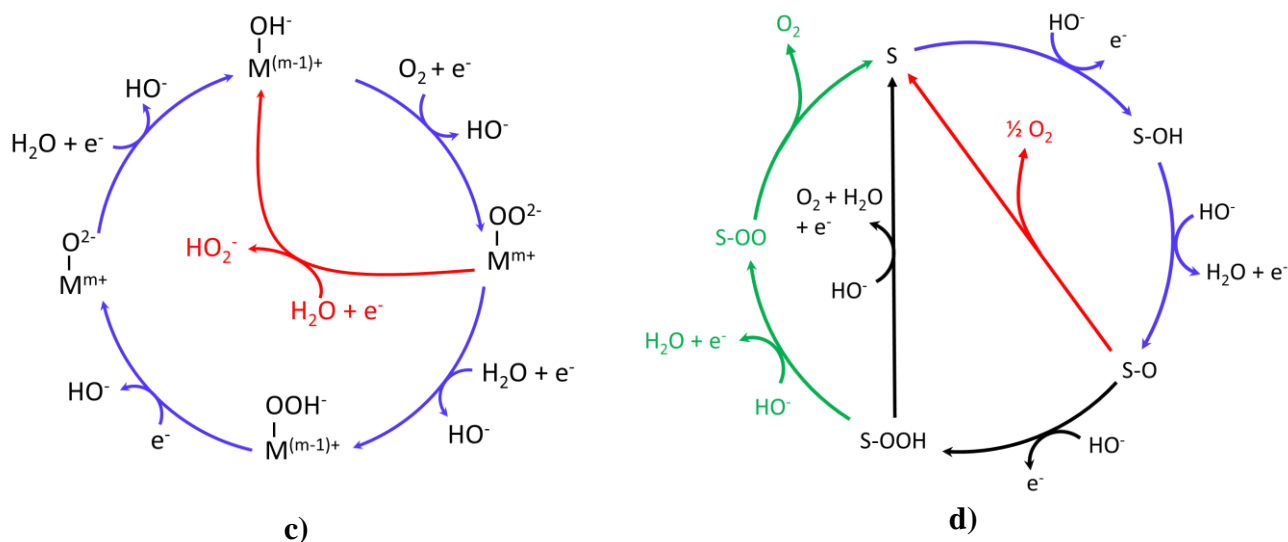
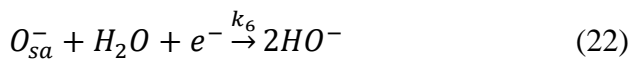
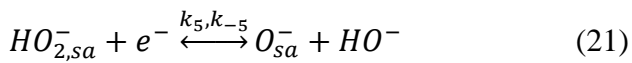
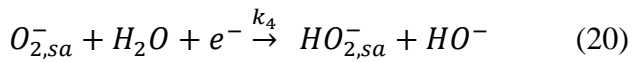
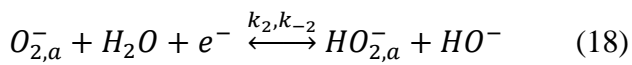


Figure 2: a) Proposed ORR mechanisms in alkaline medium at Pt-based surfaces. Reproduced from ref. [44] with permission. The subscripts sa, a, b and * respectively denote “strongly adsorbed”, “weakly adsorbed”, “bulk” and the “vicinity of the electrode” b) Proposed ORR mechanisms for metal-free catalysts. Red arrows correspond to the associative mechanism and blue arrows, to the dissociative mechanism. *S* represents the active site c) Proposed ORR mechanisms in alkaline medium at non precious transition metal-based catalysts. *M* denotes the metallic center d) Proposed OER mechanisms in alkaline medium. Different ways (symbolized by arrows with different colors) are proposed for the formation of O_2 . *S* corresponds to the active site.

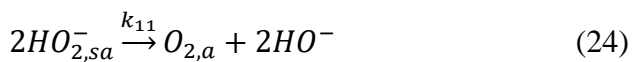
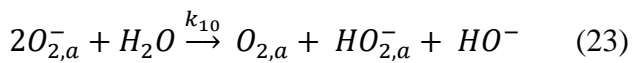
ORR mechanisms at different electrode surfaces are presented in Figure 2. The reaction mechanism may follow a pathway implying the exchange of $4e^-$ (formation of hydroxyl ion as reduction product) or a pathway accompanied by the exchange of $2e^-$ (formation of peroxide anion as reduction product). The four-electron pathway prevails for Pt-based catalysts, and the fraction of two-electron pathway often increases for non-platinum-based catalysts. Depending on O_2 adsorption mode and energy barriers, ORR can occur through different mechanisms. Adsorption mode of O_2 at the catalyst surface depends on adsorption energy, distribution of active sites as well as surface geometry [49]. To simplify, two different adsorption modes can be considered: bidentate O_2 adsorption (each O atom is coordinated to the surface) or end-on O_2 adsorption (one O atom is

coordinated to the surface). It is widely accepted that these two adsorption modes lead to a four-electron pathway and a two-electron pathway, respectively [50].

On platinum surfaces the first electron transfer step to adsorbed oxygenated species (O_{sa} resulting from the dissociation of $O_{2,a}$ or O_{2a}) is widely considered as the *rate determining step* [45] and the reaction pathways (Figure 2a) can be described using the following electrochemical equations as already reported [44, 45]:



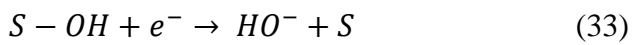
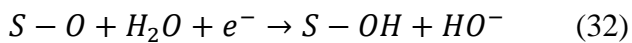
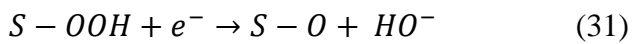
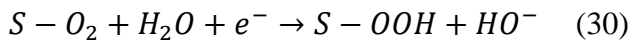
All adsorbed species may be subjected to several chemical transformations, as described by the following equations:



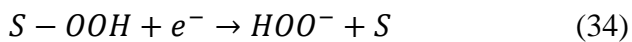
Finally, equilibria exist between weakly adsorbed species (adsorption energy in the range of kT) and strongly adsorbed species. The strength of adsorption greatly affects the rate of chemical and electrochemical steps. These equilibria can be described by the following equations:



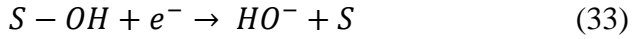
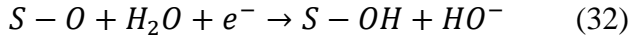
As for platinum-based catalysts, ORR at metal free surfaces can occur through associative or dissociative mechanisms (Figure 2b) [48, 51]. It was nevertheless found that the energy barrier to form adsorbed peroxide from adsorbed O_2 is lower than that corresponding to O_2 dissociation, thus associative mechanism is energetically favored [52]. Associative mechanism first involves the adsorption of molecular oxygen onto the catalyst surface and the overall reaction mechanism proceeds as follows (S represents the active site):



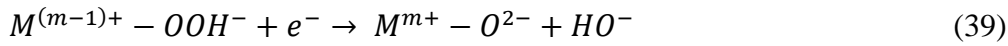
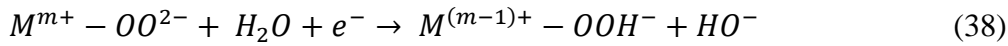
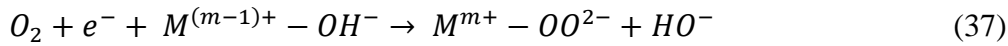
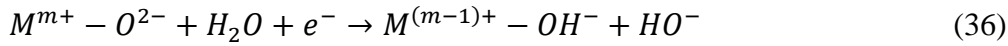
Alternatively, depending on the relative stability of $S-O$ and $S-OOH$ intermediates, $S-OOH$ may accept an electron before the releasing of peroxide anion into the electrolyte according to the following equation:



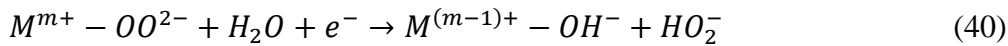
For the dissociative mechanism ORR begins with adsorption of O₂ and its further dissociation into two S-O intermediates. This reaction pathway only leads to the formation of hydroxyl ions as reduction products. This reaction pathway can be described as follows:



ORR at transition metal oxide surfaces has a quite different pathway. First, surface transition metal cations (*M*) of the oxide react with water molecules to form adsorbed OH⁻ species. The charge modification occurring subsequently to protonation of surface oxygen ligand is counterbalanced by the reduction of the metallic cation (*M*). The overall reaction process can be described as follows:



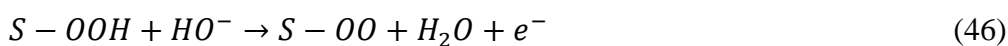
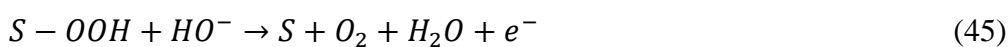
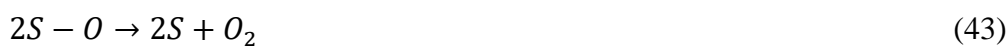
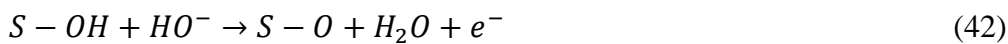
In this reaction pathway, the displacement or the regeneration of surface hydroxide can be considered as the *rate determining step* [53]. The reduction process can also lead to the formation of the two-electron product that is to know peroxide anion according to the following equation:



The uniqueness of double layer structure in alkaline medium allows modifying ORR kinetics independently on the chemical nature of the electrode. This is made possible in reason of H-bond formation between H atom of OH⁻ species at the inner Helmholtz plane and water solvating O₂ molecules located at the outer Helmholtz plane. This facilitates the outer electron transfer towards O₂ molecule leading to the formation of superoxide anions [54]. This latter phenomenon allows

compensating the possible weak interaction between O₂ and a given catalyst and consequently explains the high reduction potentials of O₂ observed for a large number of catalysts in alkaline medium. The promotion of the outer sphere electron transfer may be also responsible for the release of large amounts of peroxide species. Nevertheless, at ORR potentials, the electrostatic interaction between negatively charged peroxide anion and positively charged electrode surface could allow the fast peroxide reduction to hydroxyl ion [54].

Many research groups have proposed OER mechanisms in alkaline conditions. Some similarities and discrepancies appear in the reported studies. Most of the proposed mechanisms involve –OH as well as –O reaction intermediates and some differences are encountered in what concerns the reaction of formation of molecular O₂. These different reaction mechanisms have been proposed in Figure 2d and can be described using the following equations, where *S* denotes a general catalytic site:



As already mentioned for ORR, HER and HOR, the structure and properties of the double layer strongly influence OER kinetics. In particular, specific interactions developed between cations of the electrolyte and reaction intermediates may affect the strength of hydrogen bonds with interfacial

water. As a result, the energy required for the formation of oxygenated intermediates governing the *rate determining step* (i.e. the formation of O-O bond) is modified [55].

3.2 Catalysts for ORR/OER in alkaline medium

Numerous efficient non-noble transition metal-based hydroxides (especially Co-Fe, Ni-Fe and Ni-Co-based layered double hydroxides [47] and oxides (perovskites [56],...) with performances overcoming those of Pt-based catalysts for ORR and those of Ir- or Ru-based oxides for OER have been reported during the past few years. The ABO_3 (where A is a lanthanide or an alkaline metal and B is a transition metal) structure of perovskites is of large interest for ORR and OER since their lattice can accommodate a wide range of cations substitution both on A and B sites as well as oxygen deficiencies. Varying their composition can adjust their electronic properties and crystal structure and consequently being responsible for modifying their catalytic activity. In these structures B site is considered to be the active site for ORR/OER and their activity can be correlated with the e_g orbital filling [57]. As a result of these lattice modifications, effective materials have been designed for ORR and OER [56] (Table 2). Layered double hydroxide is also a material family which has been largely investigated in the past few years, especially for the design of efficient catalyst towards OER. These materials are composed of hexa-coordinated transition metals. Octahedrons form a two-dimensional layer by edge-sharing. The general chemical formula of layered double hydroxides is $[M_{1-x}^{2+}M_x^{3+}OH_2]^{x+}(A^{n-})_{\frac{x}{n}}.mH_2O$, where M^{2+} cations can be substituted by M^{3+} cations. The interlayer spacings are filled with anions to counterbalance the positive charge of two-dimensional layers. By exfoliating these two-dimensional materials, modifying their chemical composition of adjusting their morphology, very active OER catalysts have been designed. As an example, the high OER activity of NiFe layered double hydroxide hollow microspheres were recently reported [58]. An overpotential of only 239 mV was indeed required to reach a current density of 10 mA cm^{-2} (Table 2).

Additionally, since the amazing catalytic behavior of $\text{Co}_3\text{O}_4/\text{N-rGO}$ composites towards OER/ORR was reported in 2011 [59], studies have highlighted the design of highly efficient heterostructured catalysts for ORR/OER mainly resulting from the coupling of heteroatom-doped carbon-based materials and 3d transition metal (Co, Ni, Fe, Mn) (hydr)oxides (perovskites [60], spinels [59], layered double hydroxides [47] as recently reviewed by Chen et al. [61]. The activity and high stability of these heterostructures result from a higher dispersion degree of the oxide phase, synergistic effects as well as in some cases from the formation of a covalent heterointerface between phases notably favoring charge transfer during OER/ORR [62]. The presence of a highly active and stable oxide phase is responsible for mitigating carbon corrosion rate [61] but it is not sure it is sufficiently stable to be used in real cells. To improve stability and possibly activity of such catalysts the use of oxygen deficient oxides like TiO_{2-x} or WO_{3-x} presenting conductivities in the range of several S cm^{-1} could be of major interest [63]. In the same way, recently developed 2-D carbonitrides known as MXene could lead to very efficient heterostructures in reason of their very high electronic conductivity [64].

Oxygen vacancies at oxide surfaces can be also responsible for modifying adsorption energies of intermediates especially by tuning density of states on metal cations [65]. Another way to tune electronic properties of active sites and the to enhance ORR and/or OER electroactivity of metal oxides consists in substituting oxygen for another or several other anions resulting in the formation of very active chalcogenides [66], nitrides [67], phosphides [68] and borides [69]. These materials can be obviously coupled to an electron conductive and/or active matrix to obtain heterostructured catalysts with improved efficiency [63]. As mentioned in section 2.2, the growth of heterostructured catalysts composed of sulfides [33] or phosphides [34] directly onto Ni foam lead to the design of very efficient catalyst for overall water splitting and thus towards OER. The established interfaces with Ni oxides at OER potentials allow modifying adsorption energies of oxygenated intermediates, thus improving OER kinetics [33].

Another trend consists in developing carbon-based metal free materials in which defects and/or heteroatom are introduced to modulate electronic properties of carbon [70]. As an example, in N doped carbon-based catalysts, electronic structure of carbon atoms adjacent to N atoms (which are believed to be active sites for ORR/OER) are subject to a strong electron density modification. Pyridinic and graphitic nitrogen speciation are mainly responsible for the activity [71]. Based on these results, C₃N₄-based materials containing high amounts of nitrogen were recently investigated [72]. Other heteroatoms (S, P, B) [73] are also efficient to improve catalytic properties of carbonaceous materials. Electronic properties of doped carbon are related to the number of electrons in the external shell of the heteroatom, its electronegativity, chemical hardness and size [73]. Synthesizing multiple-doped materials is furthermore recognized as an efficient way to get an active catalyst. As an example, for nitrogen and phosphorous dual-doped carbon-based materials it was shown from DFT calculations that formation of P-N bonds and the presence of N dopants were respectively at the origin of the OER and ORR activity [74]. These theoretical considerations led to the synthesis of a highly active P/N doped graphene framework exhibiting an ORR half wave potential of 0.85 V vs. RHE and a potential of 1.55 V vs. RHE to drive a current density of 10 mA cm⁻² during OER. Another strategy consists in introducing structural defects in graphitic materials to tune carbon electronic structure. Especially, DFT calculations shown that a five-carbon ring adjacent to a seven-carbon ring leads to an optimal adsorption energy for oxygenated intermediates [75]. Based on this work, numerous catalysts were designed for OER and ORR [76]. Nevertheless, stability of carbon-based catalysts at electrode potentials, required for the OER and under harsh conditions, remains questionable. OER/ORR activities of materials described in this section are reported in Table 2

Table 2: Representative recently developed catalysts for OER/ORR in alkaline medium. Performances of reported catalysts can be systematically compared with those of reference catalysts tested under the same operating conditions. E_{1/2} represents the half-wave potential measured from

ORR polarization curves. n is the number of electrons exchanged per oxygen molecule. E_{j10} and E_{j50} corresponds to the electrode potential required to drive respective current densities of 10 and 50 mA cm^{-2} . b is the Tafel slope.

Oxygen reduction reaction	Catalyst	Morphology	Loading (mg cm ⁻²)	Working electrode	Electrolyte	E _{1/2} (V vs. RHE)	n	Ref.
	La _{0.8} Sr _{0.2} Mn _{0.6} Ni _{0.4} O ₃	Nanoparticles (14 nm)	0.14	Glassy carbon	1 M KOH	0.66 (ca. -0.4 V/ SCE)	3.92	[56]
	Pt/C	Commercial 20 wt.% Pt/C	0.028	Glassy carbon	1 M KOH	0.83 (ca. -0.24 V/ SCE)	4	
	Ba _{0.5} Sr _{0.5} Co _{0.5} Fe _{0.2} O _{3-δ} /acetylene black	Microparticles	ca. 0.4	Glassy carbon	0.1 M KOH	ca. 0.65	n/a	[60]
	MnCo ₂ O ₄ /N-rGO	Particles (5 nm) deposited onto N-rGO	0.1	Glassy carbon	1 M KOH	0.87	3.90	[62]
	Pt/C	Commercial 20 wt.% Pt/C	0.1	Glassy carbon	1 M KOH	0.89	n/a	
	ZrN	Nanoparticles (45 nm)	0.024	Glassy carbon	0.1 M KOH	0.8	3.9 - 4.0	[67]
	Pt/C	Commercial 20 wt.% Pt/C (Johnson Matthey)	0.024	Glassy carbon	0.1 M KOH	0.8	3.80	
	CoS _x @P-C ₃ N ₄ /rGO	Porous C ₃ N ₄ matrix supported onto rGO and containing CoS _x nanoparticles	0.4	Glassy carbon	0.1 M KOH	0.78	3.90	[72]
	Pt/C	Commercial 20 wt.% Pt/C	0.2	Glassy carbon	0.1 M KOH	0.81	3.90	
	P,N-doped graphene	Graphene framework	0.1	Glassy carbon	0.1 M KOH	0.85	3.99	[74]
	Pt/C	Commercial 20 wt.% Pt/C (Alfa Aesar)	0.1	Glassy carbon	0.1 M KOH	0.82	n/a	
	N,P-doped graphene/carbon fiber	P,N dual doped defective graphene interacting with carbon fibers	N/A	Glassy carbon	0.1 M KOH	0.79	3.8	[76]

	Pt/C	Commercial 20 wt.% Pt/C (Johnson Matthey)	0.2	Glassy carbon	0.1 M KOH	0.83	N/A		
Oxygen evolution reaction	Catalyst	Morphology	Loading (mg cm⁻²)	Working electrode	Electrolyte	E_{j10} (V vs. RHE)	E_{j50} (V vs. RHE)	b (mV dec⁻¹)	Ref.
	MoS ₂ /Ni ₃ S ₂ /nickel foam	Porous heterostructure grown onto Ni foam	9.7	Ni foam	1 M KOH	1.45	ca. 1.51	88	
	IrO ₂	Commercial powder (Fuel cell store)	3	Ni foam	1 M KOH	1.56	ca. 1.58	76	
	FeP/Ni ₂ P/nickel foam	Porous heterostructures composed of FeP and Ni ₂ P nanoparticles grown onto Ni foam	8	Ni foam	1 M KOH	1.39	n/a	23	
	IrO ₂	Commercial powder (Alfa Aesar)	n/a	n/a	1 M KOH	1.52	n/a	72	
	La _{0.5} Sr _{0.2} Mn _{0.6} Ni _{0.4} O ₃	Nanoparticles (14 nm)	0.14	Glassy carbon	0.1 M KOH	1.86 (0.85 V/SCE)	n/a	n/a	[56]
	Ni-Fe-layered double hydroxide	Hollow microsphere (350 nm)	0.25	Glassy carbon	1 M KOH	1.47	ca. 1.50	53	[58]
Ir/C	Commercial 20 wt.% Ir/C	0.25	Glassy carbon	1 M KOH	1.52	ca. 1.57	75		

Co ₃ O ₄ /N-rGO	Particles supported onto N-rGO (4-8 nm)	1	Ni foam	1 M KOH	1.54	1.58	67	[59]
Ba _{0.5} Sr _{0.5} Co _{0.5} Fe _{0.2} O _{3-δ} /acetylene black	Microparticles	ca. 0.4	Glassy carbon	0.1 M KOH	1.58	n/a	59	[60]
Co layered double hydroxide/Ti ₃ C ₂ T _x	Mxene covered with layered double hydroxide nanosheets	0.35	Glassy carbon	1 M KOH	1.53	n/a	82	[64]
IrO ₂	Commercial powder (Alfa Aesar)	0.35	Glassy carbon	1 M KOH	1.64	n/a	n/a	
FeCo oxide nanosheets	Nanosheets (width 400 nm - thickness 1.2 nm)	0.36	Glassy carbon	0.1 M KOH	ca. 1.54	n/a	37	[65]
RuO ₂	Commercial powder	0.36	Glassy carbon	0.1 M KOH	ca. 1.65	n/a	80	
Ni _{0.75} Fe _{0.25} -P/PO ₃ @functionnalized CNT	Ni-Fe phosphide nanoparticles (10 nm) anchored onto functionnalized carbon nanotubes	0.5	Glassy carbon	1 M KOH	ca. 1.49	1.52	45	[68]
RuO ₂	Commercial powder (Shangai Hansi chemical industry)	0.5	Glassy carbon	1 M KOH	1.55	ca. 1.65	48	
Fe-Ni-B/NF	Nanosheets (length 100 nm - a few nanometers width)	1	Ni foam	1 M KOH	1.47	ca. 1.49	38	[69]
RuO ₂ /NF	Commercial RuO ₂ powder	1	Ni foam	1 M KOH	1.52	ca. 1.57	78	
P,N dual doped graphene	Graphene frameworks	0.1	Glassy carbon	0.1 M KOH	1.55	N/A	N/A	[74]
Ir/C	Commercial 20 Wt. % Ir/C catalyst (Fuel cell store)	0.1	Glassy carbon	0.1 M KOH	ca. 1.58	N/A	N/A	

4. Conclusions and perspectives

This short review provides a full understanding of HER, HOR, OER and ORR mechanisms in alkaline electrolyte and gives an overview of state-of-the-art catalysts designed for these reactions. Even if very efficient materials have been reported during the past few years, the design of catalysts remains based on a trial and error approach. A general guideline to design efficient catalysts can be summarized in the following points: 1) engineering the porosity of the structure (microporosity, mesoporosity, macroporosity) to increase the number and density of exposed active sites as well as to improve diffusion of reactants and electrolyte 2) using a stable electron conductive substrate improving dispersion of catalysts and active sites activity by accelerating charge transfer and tuning electronic properties of active sites 3) engineering heterostructured catalysts with exposed heterointerfaces leading to the optimization of adsorption energies of reaction intermediates 4) modulating electronic properties of active sites by using a suitable heteroatom doping strategy or by inducing the formation of structural vacancies. Additionally, the better understanding of electrode/electrolyte interface in alkaline media and particularly the interaction between species (water, alkali cations,...) in the double layer and the inner-sphere HO^- adsorption is required to improve our understanding of phenomena and then to extract better rational design principles. The stability of designed catalysts should be evaluated under conditions mimicking the working environment encountered in real cells. Finally, measurements of catalysts activity should be rationalized by following already reported guidelines in order to establish unbiased comparisons between different studies.

Conflict of interest

Nothing declared

Acknowledgements: The authors are grateful to the European Union (ERDF) and “Region Nouvelle Aquitaine” for financial support.

5. References

Papers of outstanding interest, published within the past two years have been highlighted with ••.

- [1] Zou X, Zhang Y: **Noble metal-free hydrogen evolution catalysts for water splitting.** *Chem. Soc. Rev.* 2015 **44**: 5148-5180. <http://dx.doi.org/10.1039/C4CS00448E>
- [2] Varcoe JR, Slade RCT: **Prospects for Alkaline Anion-Exchange Membranes in Low Temperature Fuel Cells.** *Fuel Cells* 2005 **5**: 187-200. <http://dx.doi.org/10.1002/fuce.200400045>
- [3] Ramaswamy N, Ghoshal S, Bates MK, Jia Q, Li J, Mukerjee S: **Hydrogen oxidation reaction in alkaline media: Relationship between electrocatalysis and electrochemical double-layer structure.** *Nano Energ.* 2017 **41**: 765-771. <https://doi.org/10.1016/j.nanoen.2017.07.053>
- [4] Varcoe JR, Atanassov P, Dekel DR, Herring AM, Hickner MA, Kohl PA, Kucernak AR, Mustain WE, Nijmeijer K, Scott K, Xu T, Zhuang L: **Anion-exchange membranes in electrochemical energy systems.** *Energ. Environ. Sci.* 2014 **7**: 3135-3191. <http://dx.doi.org/10.1039/C4EE01303D>
- [5] Tafel J: Über die Polarisation bei kathodischer Wasserstoffentwicklung, *Z. Physik. Chem.*, 1905, pp. 641.
- [6] Parsons R: **The rate of electrolytic hydrogen evolution and the heat of adsorption of hydrogen.** *Trans. Faraday Soc.* 1958 **54**: 1053-1063. <http://dx.doi.org/10.1039/TF9585401053>

- [7] Durst J, Siebel A, Simon C, Hasché F, Herranz J, Gasteiger HA: **New insights into the electrochemical hydrogen oxidation and evolution reaction mechanism.** *Energ. Environ. Sci.* 2014 **7**: 2255-2260. <http://dx.doi.org/10.1039/C4EE00440J>
- [8] Rheinländer PJ, Herranz J, Durst J, Gasteiger HA: **Kinetics of the Hydrogen Oxidation/Evolution Reaction on Polycrystalline Platinum in Alkaline Electrolyte Reaction Order with Respect to Hydrogen Pressure.** *J. Electrochem. Soc.* 2014 **161**: F1448-F1457. <http://dx.doi.org/10.1149/2.0501414jes>
- [9] Sheng W, Zhuang Z, Gao M, Zheng J, Chen JG, Yan Y: **Correlating hydrogen oxidation and evolution activity on platinum at different pH with measured hydrogen binding energy.** *Nat. Commun.* 2015 **6**: 5848. <http://dx.doi.org/10.1038/ncomms6848>
- [10] McCrum IT, Janik MJ: **First Principles Simulations of Cyclic Voltammograms on Stepped Pt(553) and Pt(533) Electrode Surfaces.** *ChemElectroChem* 2016 **3**: 1609-1617. <http://dx.doi.org/10.1002/celec.201600293>
- [11] Chen X, McCrum IT, Schwarz KA, Janik MJ, Koper MTM: **Co-adsorption of Cations as the Cause of the Apparent pH Dependence of Hydrogen Adsorption on a Stepped Platinum Single-Crystal Electrode.** *Angew. Chem. Int. Ed.* 2017 **56**: 15025-15029. <http://dx.doi.org/10.1002/anie.201709455>
- [12] Strmcnik D, Lopes PP, Genorio B, Stamenkovic VR, Markovic NM: **Design principles for hydrogen evolution reaction catalyst materials.** *Nano Energ.* 2016 **29**: 29-36. <https://doi.org/10.1016/j.nanoen.2016.04.017>
- [13] Strmcnik D, Uchimura M, Wang C, Subbaraman R, Danilovic N, van der Vliet D, Paulikas AP, Stamenkovic VR, Markovic NM: **Improving the hydrogen oxidation reaction rate by promotion of hydroxyl adsorption.** *Nat. Chem.* 2013 **5**: 300-306. <http://dx.doi.org/10.1038/nchem.1574>
- [14] Liu E, Li J, Jiao L, Doan HTT, Liu Z, Zhao Z, Huang Y, Abraham KM, Mukerjee S, Jia Q: **Unifying the Hydrogen Evolution and Oxidation Reactions Kinetics in Base by**

Identifying the Catalytic Roles of Hydroxyl-Water-Cation Adducts. *J. Am. Chem. Soc.* 2019 **141**: 3232-3239. <http://dx.doi.org/10.1021/jacs.8b13228>

- This article reports for the first time the role played by hydroxyl-water-alkali metal cation adducts on HER/HOR kinetics
- [15] Campos-Roldán CA, Alonso-Vante N: **The Hydrogen Oxidation Reaction in Alkaline Medium: An Overview.** *Electrochem. Energ. Rev.* 2019 **2**: 312-331. <http://dx.doi.org/10.1007/s41918-019-00034-6>
- [16] Alesker M, Page M, Shviro M, Paska Y, Gershinsky G, Dekel DR, Zitoun D: **Palladium/nickel bifunctional electrocatalyst for hydrogen oxidation reaction in alkaline membrane fuel cell.** *J. Power Sources* 2016 **304**: 332-339. <https://doi.org/10.1016/j.jpowsour.2015.11.026>
- [17] Scofield ME, Zhou Y, Yue S, Wang L, Su D, Tong X, Vukmirovic MB, Adzic RR, Wong SS: **Role of Chemical Composition in the Enhanced Catalytic Activity of Pt-Based Alloyed Ultrathin Nanowires for the Hydrogen Oxidation Reaction under Alkaline Conditions.** *ACS Catal.* 2016 **6**: 3895-3908. <http://dx.doi.org/10.1021/acscatal.6b00350>
- [18] Miller HA, Vizza F, Marelli M, Zadick A, Dubau L, Chatenet M, Geiger S, Cherevko S, Doan H, Pavlicek RK, Mukerjee S, Dekel DR: **Highly active nanostructured palladium-ceria electrocatalysts for the hydrogen oxidation reaction in alkaline medium.** *Nano Energ.* 2017 **33**: 293-305. <https://doi.org/10.1016/j.nanoen.2017.01.051>
- [19] Sheng W, Bivens AP, Myint M, Zhuang Z, Forest RV, Fang Q, Chen JG, Yan Y: **Non-precious metal electrocatalysts with high activity for hydrogen oxidation reaction in alkaline electrolytes.** *Energ. Environ. Sci.* 2014 **7**: 1719-1724. <http://dx.doi.org/10.1039/C3EE43899F>
- [20] Zhuang Z, Giles SA, Zheng J, Jenness GR, Caratzoulas S, Vlachos DG, Yan Y: **Nickel supported on nitrogen-doped carbon nanotubes as hydrogen oxidation reaction**

catalyst in alkaline electrolyte. *Nat. Commun.* 2016 **7**: 10141.

<http://dx.doi.org/10.1038/ncomms10141>

- [21] Ni W, Krammer A, Hsu C-S, Chen HM, Schüler A, Hu X: **Ni₃N as an Active Hydrogen Oxidation Reaction Catalyst in Alkaline Medium.** *Angew. Chem. Int. Ed.* 2019 **58**: 7445-7449. <http://dx.doi.org/10.1002/anie.201902751>
- This article deals with the synthesis and characterization of Ni₃N/C catalyst exhibiting the highest HOR activity ever reported for a non-noble metal-based material in alkaline medium. A downshift of the Ni d-band as well as and interfacial charge transfer from Ni₃N to carbon are responsible for the weakening of binding energies of hydrogenated and oxygenated intermediates.
- [22] Lao M, Rui K, Zhao G, Cui P, Zheng X, Dou SX, Sun W: **Platinum/Nickel Bicarbonate Heterostructures towards Accelerated Hydrogen Evolution under Alkaline Conditions.** *Angew. Chem. Int. Ed.* 2019 **58**: 5432-5437. <http://dx.doi.org/10.1002/anie.201901010>
- [23] Huang Y, Gong Q, Song X, Feng K, Nie K, Zhao F, Wang Y, Zeng M, Zhong J, Li Y: **Mo₂C Nanoparticles Dispersed on Hierarchical Carbon Microflowers for Efficient Electrocatalytic Hydrogen Evolution.** *ACS Nano* 2016 **10**: 11337-11343. <http://dx.doi.org/10.1021/acsnano.6b06580>
- [24] Hao Z, Yang S, Niu J, Fang Z, Liu L, Dong Q, Song S, Zhao Y: **A bimetallic oxide Fe_{1.89}Mo_{4.11}O₇ electrocatalyst with highly efficient hydrogen evolution reaction activity in alkaline and acidic media.** *Chem. Sci.* 2018 **9**: 5640-5645. <http://dx.doi.org/10.1039/C8SC01710G>
- [25] Kuang P, Tong T, Fan K, Yu J: **In Situ Fabrication of Ni–Mo Bimetal Sulfide Hybrid as an Efficient Electrocatalyst for Hydrogen Evolution over a Wide pH Range.** *ACS Catal.* 2017 **7**: 6179-6187. <http://dx.doi.org/10.1021/acscatal.7b02225>
- [26] Yang J, Lei C, Wang H, Yang B, Li Z, Qiu M, Zhuang X, Yuan C, Lei L, Hou Y, Feng X: **High-index faceted binary-metal selenide nanosheet arrays as efficient 3D electrodes**

- for alkaline hydrogen evolution. *Nanoscale* 2019 **11**: 17571-17578.
<http://dx.doi.org/10.1039/C9NR06976C>
- [27] Zhang Y, Liu Y, Ma M, Ren X, Liu Z, Du G, Asiri AM, Sun X: **A Mn-doped Ni₂P nanosheet array: an efficient and durable hydrogen evolution reaction electrocatalyst in alkaline media.** *Chemical Communications* 2017 **53**: 11048-11051.
<http://dx.doi.org/10.1039/C7CC06278H>
- [28] Lai J, Huang B, Chao Y, Chen X, Guo S: **Strongly Coupled Nickel–Cobalt Nitrides/Carbon Hybrid Nanocages with Pt-Like Activity for Hydrogen Evolution Catalysis.** *Adv. Mater.* 2019 **31**: 1805541. <http://dx.doi.org/10.1002/adma.201805541>
- [29] Sheng M, Wu Q, Wang Y, Liao F, Zhou Q, Hou J, Weng W: **Network-like porous Co-Ni-B grown on carbon cloth as efficient and stable catalytic electrodes for hydrogen evolution.** *Electrochem. Commun.* 2018 **93**: 104-108.
<https://doi.org/10.1016/j.elecom.2018.06.017>
- [30] Peng Z, Yang S, Jia D, Da P, He P, Al-Enizi AM, Ding G, Xie X, Zheng G: **Homologous metal-free electrocatalysts grown on three-dimensional carbon networks for overall water splitting in acidic and alkaline media.** *J. Mater. Chem. A* 2016 **4**: 12878-12883.
<http://dx.doi.org/10.1039/C6TA04426C>
- [31] Subbaraman R, Tripkovic D, Strmcnik D, Chang K-C, Uchimura M, Paulikas AP, Stamenkovic V, Markovic NM: **Enhancing Hydrogen Evolution Activity in Water Splitting by Tailoring Li⁺-Ni(OH)₂-Pt Interfaces.** *Science* 2011 **334**: 1256-1260.
<http://dx.doi.org/10.1126/science.1211934>
- [32] Li S, Cheng C, Sagaltchik A, Pachfule P, Zhao C, Thomas A: **Metal-Organic Precursor-Derived Mesoporous Carbon Spheres with Homogeneously Distributed Molybdenum Carbide/Nitride Nanoparticles for Efficient Hydrogen Evolution in Alkaline Media.** *Adv. Funct. Mater.* 2019 **29**: 1807419. <http://dx.doi.org/10.1002/adfm.201807419>

- [33] Zhang J, Wang T, Pohl D, Rellinghaus B, Dong R, Liu S, Zhuang X, Feng X: **Interface Engineering of MoS₂/Ni₃S₂ Heterostructures for Highly Enhanced Electrochemical Overall-Water-Splitting Activity.** *Angew. Chem. Int. Ed.* 2016 **55**: 6702-6707. <http://dx.doi.org/10.1002/anie.201602237>
- [34] Yu F, Zhou H, Huang Y, Sun J, Qin F, Bao J, Goddard WA, Chen S, Ren Z: **High-performance bifunctional porous non-noble metal phosphide catalyst for overall water splitting.** *Nat. Commun.* 2018 **9**: 2551. <http://dx.doi.org/10.1038/s41467-018-04746-z>
- This article deals with the synthesis and characterization of a Fe/PNi₂P heterostructured catalyst directly grown onto a Ni foam. This material is one of the most efficient catalysts reported to date for overall water splitting.
- [35] Huang Y, Sun Y, Zheng X, Aoki T, Pattengale B, Huang J, He X, Bian W, Younan S, Williams N, Hu J, Ge J, Pu N, Yan X, Pan X, Zhang L, Wei Y, Gu J: **Atomically engineering activation sites onto metallic 1T-MoS₂ catalysts for enhanced electrochemical hydrogen evolution.** *Nat. Commun.* 2019 **10**: 982. <http://dx.doi.org/10.1038/s41467-019-08877-9>
- [36] Wu Y, Liu X, Han D, Song X, Shi L, Song Y, Niu S, Xie Y, Cai J, Wu S, Kang J, Zhou J, Chen Z, Zheng X, Xiao X, Wang G: **Electron density modulation of NiCo₂S₄ nanowires by nitrogen incorporation for highly efficient hydrogen evolution catalysis.** *Nat. Commun.* 2018 **9**: 1425. <http://dx.doi.org/10.1038/s41467-018-03858-w>
- [37] Ling T, Zhang T, Ge B, Han L, Zheng L, Lin F, Xu Z, Hu W-B, Du X-W, Davey K, Qiao S-Z: **Well-Dispersed Nickel- and Zinc-Tailored Electronic Structure of a Transition Metal Oxide for Highly Active Alkaline Hydrogen Evolution Reaction.** *Adv. Mater.* 2019 **31**: 1807771. <http://dx.doi.org/10.1002/adma.201807771>
- [38] Busch M, Halck NB, Kramm UI, Siahrostami S, Krttil P, Rossmeisl J: **Beyond the top of the volcano? – A unified approach to electrocatalytic oxygen reduction and oxygen evolution.** *Nano Energy* 2016 **29**: 126-135. <https://doi.org/10.1016/j.nanoen.2016.04.011>

- [39] Govindarajan N, García-Lastra JM, Meijer EJ, Calle-Vallejo F: **Does the breaking of adsorption-energy scaling relations guarantee enhanced electrocatalysis?** *Curr. Opin. Electrochem.* 2018 **8**: 110-117. <https://doi.org/10.1016/j.coelec.2018.03.025>
- This study reports that breaking scaling relations is not enough to improve ORR/OER activity of a catalyst. It is required to take into account another descriptor: electrochemical step symmetry index.
- [40] Koper MTM: **Thermodynamic theory of multi-electron transfer reactions: Implications for electrocatalysis.** *J. Electroanal. Chem.* 2011 **660**: 254-260. <https://doi.org/10.1016/j.jelechem.2010.10.004>
- [41] Rossmeisl J, Qu ZW, Zhu H, Kroes GJ, Nørskov JK: **Electrolysis of water on oxide surfaces.** *J. Electroanal. Chem.* 2007 **607**: 83-89. <http://dx.doi.org/10.1016/j.jelechem.2006.11.008>
- [42] Govindarajan N, Koper MTM, Meijer EJ, Calle-Vallejo F: **Outlining the Scaling-Based and Scaling-Free Optimization of Electrocatalysts.** *ACS Catal.* 2019 **9**: 4218-4225. <http://dx.doi.org/10.1021/acscatal.9b00532>
- This study is a guideline for the rational design of optimized electrocatalysts based on the introduction of two parameters into the activity descriptor: a classically used scaling-based parameter and an unconventional scaling-free parameter.
- [43] Briquet LGV, Sarwar M, Mugo J, Jones G, Calle-Vallejo F: **A New Type of Scaling Relations to Assess the Accuracy of Computational Predictions of Catalytic Activities Applied to the Oxygen Evolution Reaction.** *ChemCatChem* 2017 **9**: 1261-1268. <http://dx.doi.org/10.1002/cctc.201601662>
- [44] Anastasijević NA, Vesović V, Adžić RR: **Determination of the kinetic parameters of the oxygen reduction reaction using the rotating ring-disk electrode: Part I. Theory.** *J. Electroanal. Chem.* 1987 **229**: 305-316. [https://doi.org/10.1016/0022-0728\(87\)85148-3](https://doi.org/10.1016/0022-0728(87)85148-3)

- [45] Ge X, Sumboja A, Wu D, An T, Li B, Goh FWT, Hor TSA, Zong Y, Liu Z: **Oxygen Reduction in Alkaline Media: From Mechanisms to Recent Advances of Catalysts.** *ACS Catal.* 2015 **5**: 4643-4667. <https://doi.org/10.1021/acscatal.5b00524>
- [46] Suen N-T, Hung S-F, Quan Q, Zhang N, Xu Y-J, Chen HM: **Electrocatalysis for the oxygen evolution reaction: recent development and future perspectives.** *Chem. Soc. Rev.* 2017 **46**: 337-365. <https://doi.org/10.1039/C6CS00328A>
- [47] Cai Z, Bu X, Wang P, Ho JC, Yang J, Wang X: **Recent advances in layered double hydroxide electrocatalysts for the oxygen evolution reaction.** *J. Mater. Chem. A* 2019 **7**: 5069-5089. <https://doi.org/10.1039/C8TA11273H>
- [48] Li Y, Li Q, Wang H, Zhang L, Wilkinson DP, Zhang J: **Recent Progresses in Oxygen Reduction Reaction Electrocatalysts for Electrochemical Energy Applications.** *Electrochem. Energ. Rev.* 2019 **2**: 518-538. <https://doi.org/10.1007/s41918-019-00052-4>
- [49] Cheng F, Chen J: **Metal-air batteries: from oxygen reduction electrochemistry to cathode catalysts.** *Chem. Soc. Rev.* 2012 **41**: 2172-2192. <https://doi.org/10.1039/C1CS15228A>
- [50] Jörissen L: **Bifunctional oxygen/air electrodes.** *J. Power Sources* 2006 **155**: 23-32. <https://doi.org/10.1016/j.jpowsour.2005.07.038>
- [51] Ma R, Lin G, Zhou Y, Liu Q, Zhang T, Shan G, Yang M, Wang J: **A review of oxygen reduction mechanisms for metal-free carbon-based electrocatalysts.** *npj Comput. Mater.* 2019 **5**: 78. <http://dx.doi.org/10.1038/s41524-019-0210-3>
- [52] Yu L, Pan X, Cao X, Hu P, Bao X: **Oxygen reduction reaction mechanism on nitrogen-doped graphene: A density functional theory study.** *J. Catal.* 2011 **282**: 183-190. <https://doi.org/10.1016/j.jcat.2011.06.015>
- [53] Suntivich J, Gasteiger HA, Yabuuchi N, Nakanishi H, Goodenough JB, Shao-Horn Y: **Design principles for oxygen-reduction activity on perovskite oxide catalysts for fuel**

- cells and metal–air batteries. *Nat. Chem.* 2011 **3**: 546-550.
<https://doi.org/10.1038/nchem.1069>
- [54] He Q, Cairns EJ: **Review—Recent Progress in Electrocatalysts for Oxygen Reduction Suitable for Alkaline Anion Exchange Membrane Fuel Cells.** *J. Electrochem. Soc.* 2015 **162**: F1504-F1539. <https://doi.org/10.1149/2.0551514jes>
- [55] Yang C, Fontaine O, Tarascon J-M, Grimaud A: **Chemical Recognition of Active Oxygen Species on the Surface of Oxygen Evolution Reaction Electrocatalysts.** *Angew. Chem. Int. Ed.* 2017 **56**: 8652-8656. <http://dx.doi.org/10.1002/anie.201701984>
- [56] Wang Z, You Y, Yuan J, Yin Y-X, Li Y-T, Xin S, Zhang D: **Nickel-Doped $\text{La}_{0.8}\text{Sr}_{0.2}\text{Mn}_{1-x}\text{Ni}_x\text{O}_3$ Nanoparticles Containing Abundant Oxygen Vacancies as an Optimized Bifunctional Catalyst for Oxygen Cathode in Rechargeable Lithium–Air Batteries.** *ACS Appl. Mater. Int.* 2016 **8**: 6520-6528. <https://doi.org/10.1021/acsami.6b00296>
- [57] Xu J, Chen C, Han Z, Yang Y, Li J, Deng Q: **Recent Advances in Oxygen Electrocatalysts Based on Perovskite Oxides.** *Nanomater.* 2019 **9**: 1161.
<http://dx.doi.org/10.3390/nano908116>
- [58] Zhang C, Shao M, Zhou L, Li Z, Xiao K, Wei M: **Hierarchical NiFe Layered Double Hydroxide Hollow Microspheres with Highly-Efficient Behavior toward Oxygen Evolution Reaction.** *ACS Appl. Mater. Int.* 2016 **8**: 33697-33703.
<http://dx.doi.org/10.1021/acsami.6b12100>
- [59] Liang Y, Li Y, Wang H, Zhou J, Wang J, Regier T, Dai H: **Co_3O_4 nanocrystals on graphene as a synergistic catalyst for oxygen reduction reaction.** *Nat. Mater.* 2011 **10**: 780-786. <http://dx.doi.org/10.1038/nmat3087>
- [60] Fabbri E, Nachttegaal M, Cheng X, Schmidt TJ: **Superior Bifunctional Electrocatalytic Activity of $\text{Ba}_{0.5}\text{Sr}_{0.5}\text{Co}_{0.8}\text{Fe}_{0.2}\text{O}_{3-\delta}$ /Carbon Composite Electrodes: Insight into the Local Electronic Structure.** *Adv. Energ. Mater.* 2015 **5**: 1402033.
<https://doi.org/10.1002/aenm.201402033>

- [61] Chen M, Wang L, Yang H, Zhao S, Xu H, Wu G: **Nanocarbon/oxide composite catalysts for bifunctional oxygen reduction and evolution in reversible alkaline fuel cells: A mini review.** *J. Power Sources* 2018 **375**: 277-290. <https://doi.org/10.1016/j.jpowsour.2017.08.062>
- [62] Liang Y, Wang H, Zhou J, Li Y, Wang J, Regier T, Dai H: **Covalent Hybrid of Spinel Manganese–Cobalt Oxide and Graphene as Advanced Oxygen Reduction Electrocatalysts.** *J. Am. Chem. Soc.* 2012 **134**: 3517-3523. <http://dx.doi.org/10.1021/ja210924t>
- [63] Ibrahim KB, Tsai M-C, Chala SA, Berihun MK, Kahsay AW, Berhe TA, Su W-N, Hwang B-J: **A review of transition metal-based bifunctional oxygen electrocatalysts.** *J. Chin. Chem. Soc.* 2019 **66**: 829-865. <http://dx.doi.org/10.1002/jccs.201900001>
- [64] Benchakar M, Bilyk T, Garnero C, Loupias L, Morais C, Pacaud J, Canaff C, Chartier P, Morisset S, Guignard N, Mauchamp V, C  lerier S, Habrioux A: **MXene Supported Cobalt Layered Double Hydroxide Nanocrystals: Facile Synthesis Route for a Synergistic Oxygen Evolution Reaction Electrocatalyst.** *Adv. Mater. Int.* 2019 **6**: 1901328. <https://doi.org/10.1002/admi.201901328>
- [65] Zhuang L, Ge L, Yang Y, Li M, Jia Y, Yao X, Zhu Z: **Ultrathin Iron-Cobalt Oxide Nanosheets with Abundant Oxygen Vacancies for the Oxygen Evolution Reaction.** *Adv. Mater.* 2017 **29**: 1606793. <http://dx.doi.org/10.1002/adma.201606793>
- [66] Dong B, Zhao X, Han G-Q, Li X, Shang X, Liu Y-R, Hu W-H, Chai Y-M, Zhao H, Liu C-G: **Two-step synthesis of binary Ni–Fe sulfides supported on nickel foam as highly efficient electrocatalysts for the oxygen evolution reaction.** *J. Mater. Chem. A* 2016 **4**: 13499-13508. <http://dx.doi.org/10.1039/C6TA03177C>
- [67] Yuan Y, Wang J, Adimi S, Shen H, Thomas T, Ma R, Attfield JP, Yang M: **Zirconium nitride catalysts surpass platinum for oxygen reduction.** *Nat. Mater.* 2019. <http://dx.doi.org/10.1038/s41563-019-0535-9>

- In this study a zirconium nitride catalyst exhibiting an ORR activity similar to that of platinum both with a largely better stability is reported.
- [68] Huang C, Zou Y, Ye Y-Q, Ouyang T, Xiao K, Liu Z-Q: **Unveiling the active sites of Ni-Fe phosphide/metaphosphate for efficient oxygen evolution under alkaline conditions.** *Chem. Commun.* 2019 **55**: 7687-7690. <http://dx.doi.org/10.1039/C9CC03024G>
- [69] Nsanzimana JMV, Reddu V, Peng Y, Huang Z, Wang C, Wang X: **Ultrathin Amorphous Iron-Nickel Boride Nanosheets for Highly Efficient Electrocatalytic Oxygen Production.** *Chem. Eur. J.* 2018 **24**: 18502-18511. <http://dx.doi.org/10.1002/chem.201802092>
- [70] Liu X, Dai L: **Carbon-based metal-free catalysts.** *Nat. Rev. Mater.* 2016 **1**: 16064. <http://dx.doi.org/10.1038/natrevmats.2016.64>
- [71] Guo D, Shibuya R, Akiba C, Saji S, Kondo T, Nakamura J: **Active sites of nitrogen-doped carbon materials for oxygen reduction reaction clarified using model catalysts.** *Science* 2016 **351**: 361-365. <http://dx.doi.org/10.1126/science.aad0832>
- [72] Niu W, Li Z, Marcus K, Zhou L, Li Y, Ye R, Liang K, Yang Y: **Surface-Modified Porous Carbon Nitride Composites as Highly Efficient Electrocatalyst for Zn-Air Batteries.** *Adv. Energ. Mater.* 2018 **8**: 1701642. <http://dx.doi.org/10.1002/aenm.201701642>
- [73] Daems N, Sheng X, Vankelecom IFJ, Pescarmona PP: **Metal-free doped carbon materials as electrocatalysts for the oxygen reduction reaction.** *J. Mater. Chem. A* 2014 **2**: 4085-4110. <http://dx.doi.org/10.1039/c3ta14043a>
- [74] Chai G-L, Qiu K, Qiao M, Titirici M-M, Shang C, Guo Z: **Active sites engineering leads to exceptional ORR and OER bifunctionality in P,N Co-doped graphene frameworks.** *Energ. Environ. Sci.* 2017 **10**: 1186-1195. <http://dx.doi.org/10.1039/C6EE03446B>
- [75] Tang C, Wang H-F, Chen X, Li B-Q, Hou T-Z, Zhang B, Zhang Q, Titirici M-M, Wei F: **Topological Defects in Metal-Free Nanocarbon for Oxygen Electrocatalysis.** *Adv. Mater.* 2016 **28**: 6845-6851. <http://dx.doi.org/10.1002/adma.201601406>

- [76] Hang C, Zhang J, Zhu J, Li W, Kou Z, Huang Y: **In Situ Exfoliating and Generating Active Sites on Graphene Nanosheets Strongly Coupled with Carbon Fiber toward Self-Standing Bifunctional Cathode for Rechargeable Zn–Air Batteries.** *Adv. Energ. Mater.* 2018 **8**: 1703539. <http://dx.doi.org/10.1002/aenm.201703539>

Table 1: Non-exhaustive list presenting representative recently developed catalysts for HER/HOR in alkaline medium. j_0 represents the exchange current density. It has been normalized using either platinum active surface area (in that case the unit is denoted as $\text{mg cm}^{-2}_{\text{Pt}}$) or using geometric surface area. The mass normalized j_0 value is also given for HOR catalysts. η represents the overpotential. For HER, overpotential values at -10 mA cm^{-2} (η_{-10}) as well as at -100 mA cm^{-2} (η_{-100}) are given. b is the Tafel slope

Hydrogen oxidation reaction (HOR)	Catalyst	Morphology / structure	Loading ($\text{mg}_{\text{metal}} \text{cm}^{-2}$)	Working electrode	Electrolyte	j_0 ($\text{mA mg}^{-1}_{\text{metal}}$)	j_0 (mA cm^{-2})
	Pt	Nanowires	0.02	Vulcan XC 72 R coated glassy carbon	0.1 M KOH	$16 \text{ mA mg}^{-1}_{\text{Pt}}$	0.229 mA cm^{-2}
	PtRu	Nanowires	0.02	Vulcan XC 72 R coated glassy carbon	0.1 M KOH	$32 \text{ mA mg}^{-1}_{\text{Pt}}$	0.493 mA cm^{-2}
	PtFe	Nanowires	0.02	Vulcan XC 72 R coated glassy carbon	0.1 M KOH	$27 \text{ mA mg}^{-1}_{\text{Pt}}$	0.459 mA cm^{-2}
	CoMoNi	Electroplated material	n/a	Au	0.1 M KOH	n/a	0.015
	Pt	polycrystalline disk	n/a	Pt	0.1 M KOH	n/a	0.61
	Ni/N-CNT	Nanoparticles (20 nm)	0.25	Glassy carbon	0.1 M KOH	3.5	0.028
	$\text{Ni}_3\text{N/C}$	Nanoparticles (4.6 nm)	0.16	Glassy carbon	0.1 M KOH	12	0.014
Hydrogen evolution reaction (HER)	Catalyst	Morphology / structure	Loading (mg cm^{-2})	Working electrode	Electrolyte	η_{-10} (mV)	η_{-100} (mV)
	$\text{Pt/Ni}(\text{HCO}_3)_2$	20 wt. % Pt nanoparticles (2-3 nm) on $\text{Ni}(\text{HCO}_3)_2$ nanoplates	0.04	Glassy carbon	1 M KOH	-27	ca. -70 mV
	Pt	Bare Pt nanoparticles	0.2	Glassy carbon	1 M KOH	-44	ca. -125 mV
	Pt/C	Commercial 10 wt.% Pt/C (Sigma-Aldrich)	0.02	Glassy carbon	1 M KOH	ca. -50	n/a
	$\text{Mo}_2\text{C/N-doped carbon microflowers}$	N-doped microflowers consisting of nanoflakes decorated with $\beta\text{-Mo}_2\text{C}$ (particles)	0.28	Glassy carbon	1 M KOH	-100	n/a
	Pt/C	Commercial 20 wt. % Pt/C	0.28	Glassy carbon	1 M KOH	-50	n/a
	$\text{Fe}_{1.89}\text{Mo}_{4.11}\text{O}_7$	Microparticles	2.4	Bare carbon paste	1 M KOH	-197	n/a
	Pt/C	Commercial 20 wt. % Pt/C	n/a	n/a	1 M KOH	-103	n/a
	$\text{NiS}_2/\text{MoS}_2$	Hybrid porous nanowires composed of MoS_2 nanoplates and NiS_2 particles with heterojunctions	0.2	Glassy carbon	1 M KOH	-204	n/a
	Pt/C	n/a	0.2	Glassy carbon	1 M KOH	-50	n/a
	$\text{FeNiSe/exfoliated graphene}$	Mesoporous FeNiSe nanosheets grown onto exfoliated graphene	3.3	Graphite foil	1 M KOH	-187	n/a
	Pt/C	Commercial catalyst	3.3	n/a	1 M KOH	ca.-75	n/a
	Mn-doped Ni_2P	Mn-doped Ni_2P Nanosheets array on Ni foam	n/a	Ni foam	1 M KOH	ca. 50	ca. -220 mV
	Pt/C	Commercial 20 wt. % Pt/C (Sigma-Aldrich)	7.0	Ni foam	1 M KOH	ca. 20	ca. -120 mV
	NiCoN/C	Hybrid nanocages composed of nanosheets with a thickness of 2-3 nm	0.2	Glassy carbon	1 M KOH	-103	n/a
	Pt/C	Commercial Pt/C	0.05	Glassy carbon	1 M KOH	-91	n/a
	Co-Ni-B/carbon cloth	Co-Ni-B nanoparticles (5-10 nm)	0.34	Carbon cloth	1 M KOH	-80	ca. -250 mV
	Pt/C	Commercial Pt/C	0.34	Carbon cloth	1 M KOH	ca. -25	ca. -240 mV
S-doped $\text{C}_3\text{N}_4/\text{carbon naotubes/carbon}$	Fibers decorated with S-doped C_3N_4	0.5	Carbon fiber	1 M KOH	-131	ca. -250 mV	

fiber						
Mo ₂ C/Mo ₂ N	Mesoporous material	0.38	Glassy carbon	1 M KOH	-145	-222
Pt/C	20 wt. % Pt/C (Alfa Aesar)	0.38	Glassy carbon	1 M KOH	-60	-263
MoS ₂ /Ni ₃ S ₂ /nickel foam	Porous heterostructure grown onto Ni foam	9.7	Ni foam	1 M KOH	ca. -110	n/a
Pt/C	20 wt. % Pt/C (Fuel Cell store)	0.8	Ni foam	1 M KOH	ca. -25	n/a
FeP/Ni ₂ P/nickel foam	Porous heterostructures composed of FeP and Ni ₂ P nanoparticles grown onto Ni foam	8	Ni foam	1 M KOH	-14	ca. -132
Pt	Pt wire	n/a	n/a	1 M KOH	-59	ca. -132
N-NiCo ₂ S ₄	Nanowires	n/a	Ni foam	1 M KOH	-41	ca. -142
Pt/C	Commercial 20 wt. % Pt/C	2.3	Ni foam	1 M KOH	-28	ca. -142
Ni, Zn-doped CoO	Nanorods	0.486	Carbon fiber paper	1 M KOH	-53	ca. -162
Pt/C	Commercial 20 wt. % Pt/C (Fuel cell store)	0.4	Carbon fiber paper	1 M KOH	ca. -60	ca. -172
NiO@1T-MoS ₂ /CFP	Nanosheets	1.02	Carbon fiber paper	1 M KOH	-46	ca. -122
Pt/C	Commercial 20 wt. % Pt/C (Johnson Matthey)	1	Carbon fiber paper	1 M KOH	-23	ca. -132

Table 2: Representative recently developed catalysts for OER/ORR in alkaline medium. Performances of reported catalysts can be systematically compared with those of reference catalysts tested under the same operating conditions. $E_{1/2}$ represents the half-wave potential measured from ORR polarization curves. n is the number of electrons exchanged per oxygen molecule. E_{j10} and E_{j50} corresponds to the electrode potential required to drive respective current densities of 10 and 50 mA cm^{-2} . b is the Tafel slope

Oxygen reduction reaction	Catalyst	Morphology	Loadin g (mg cm ⁻²)	Workin g electrod e	Electrolyt e	E _{1/2} (V vs. RHE)	n	Ref .
	La _{0.8} Sr _{0.2} Mn _{0.6} Ni _{0.4} O ₃	Nanoparticles (14 nm)	0.14	Glassy carbon	1 M KOH	0.66 (ca. - 0.4 V/ SCE)	3.92	[56]
	Pt/C	Commercial 20 wt.% Pt/C	0.028	Glassy carbon	1 M KOH	0.83 (ca. - 0.24 V/ SCE)	4	
	Ba _{0.5} Sr _{0.5} Co _{0.5} Fe _{0.2} O _{3-δ} /acetylene black	Microparticles	ca. 0.4	Glassy carbon	0.1 M KOH	ca. 0.65	n/a	[60]
	MnCo ₂ O ₄ /N-rGO	Particles (5 nm) deposited onto N-rGO	0.1	Glassy carbon	1 M KOH	0.87	3.90	[62]
	Pt/C	Commercial 20 wt.% Pt/C	0.1	Glassy carbon	1 M KOH	0.89	n/a	
	ZrN	Nanoparticles (45 nm)	0.024	Glassy carbon	0.1 M KOH	0.8	3.9 - 4.0	[67]
	Pt/C	Commercial 20 wt.% Pt/C (Johnson Matthey)	0.024	Glassy carbon	0.1 M KOH	0.8	3.80	
	CoS _x @P-C ₃ N ₄ /rGO	Porous C ₃ N ₄ matrix supported onto rGO and containing CoS _x nanoparticles	0.4	Glassy carbon	0.1 M KOH	0.78	3.90	[72]
	Pt/C	Commercial 20 wt.% Pt/C	0.2	Glassy carbon	0.1 M KOH	0.81	3.90	[74]
P,N-doped graphene	Graphene framework	0.1	Glassy carbon	0.1 M KOH	0.85	3.99		
Pt/C	Commercial 20 wt.% Pt/C (Alfa Aesar)	0.1	Glassy carbon	0.1 M KOH	0.82	n/a		

	N,P-doped graphene/carbon fiber	P,N dual doped defective graphene interacting with carbon fibers	N/A	Glassy carbon	0.1 M KOH	0.79	3.8	[76]	
	Pt/C	Commercial 20 wt.% Pt/C (Johnson Matthey)	0.2	Glassy carbon	0.1 M KOH	0.83	N/A		
Oxygen evolution reaction	Catalyst	Morphology	Loadin g (mg cm⁻²)	Workin g electrod e	Electrolyt e	E_{j10} (V vs. RHE)	E_{j50} (V vs. RHE)	b (m V dec⁻¹)	Ref .
	MoS ₂ /Ni ₃ S ₂ /nickel foam	Porous heterostructure grown onto Ni foam	9.7	Ni foam	1 M KOH	1.45	ca. 1.51	88	
	IrO ₂	Commercial powder (Fuel cell store)	3	Ni foam	1 M KOH	1.56	ca. 1.58	76	
	FeP/Ni ₂ P/nickel foam	Porous heterostructure composed of FeP and Ni ₂ P nanoparticles grown onto Ni foam	8	Ni foam	1 M KOH	1.39	n/a	23	
	IrO ₂	Commercial powder (Alfa	n/a	n/a	1 M KOH	1.52	n/a	72	

		Aesar)							
	$\text{La}_{0.5}\text{Sr}_{0.2}\text{Mn}_{0.6}\text{Ni}_{0.4}\text{O}_3$	Nanoparticles (14 nm)	0.14	Glassy carbon	0.1 M KOH	1.86 (0.85 V/SCE)	n/a	n/a	[56]
	Ni-Fe-layered double hydroxide	Hollow microsphere (350 nm)	0.25	Glassy carbon	1 M KOH	1.47	ca. 1.50	53	[58]
	Ir/C	Commercial 20 wt.% Ir/C	0.25	Glassy carbon	1 M KOH	1.52	ca. 1.57	75	
	$\text{Co}_3\text{O}_4/\text{N-rGO}$	Particles supported onto N-rGO (4-8 nm)	1	Ni foam	1 M KOH	1.54	1.58	67	[59]
	$\text{Ba}_{0.5}\text{Sr}_{0.5}\text{Co}_{0.5}\text{Fe}_{0.2}\text{O}_{3-6}$ /acetylene black	Microparticles	ca. 0.4	Glassy carbon	0.1 M KOH	1.58	n/a	59	[60]
	Co layered double hydroxide/ $\text{Ti}_3\text{C}_2\text{T}_x$	Mxene covered with layered double hydroxide nanosheets	0.35	Glassy carbon	1 M KOH	1.53	n/a	82	[64]
	IrO_2	Commercial powder (Alfa Aesar)	0.35	Glassy carbon	1 M KOH	1.64	n/a	n/a	
	FeCo oxide nanosheets	Nanosheets (width 400 nm - thickness 1.2 nm)	0.36	Glassy carbon	0.1 M KOH	ca. 1.54	n/a	37	[65]
	RuO_2	Commercial powder	0.36	Glassy carbon	0.1 M KOH	ca. 1.65	n/a	80	
	$\text{Ni}_{0.75}\text{Fe}_{0.25}$ - P/ PO_3 @functionalize d CNT	Ni-Fe phosphide nanoparticles (10 nm) anchored onto	0.5	Glassy carbon	1 M KOH	ca. 1.49	1.52	45	[68]

		functionalized carbon nanotubes							
	RuO ₂	Commercial powder (Shanghai Hansi chemical industry)	0.5	Glassy carbon	1 M KOH	1.55	ca. 1.65	48	
	Fe-Ni-B/NF	Nanosheets (length 100 nm - a few nanometers width)	1	Ni foam	1 M KOH	1.47	ca. 1.49	38	[69]
	RuO ₂ /NF	Commercial RuO ₂ powder	1	Ni foam	1 M KOH	1.52	ca. 1.57	78	
	P,N dual doped graphene	Graphene frameworks	0.1	Glassy carbon	0.1 M KOH	1.55	N/A	N/A	
	Ir/C	Commercial 20 Wt. % Ir/C catalyst (Fuel cell store)	0.1	Glassy carbon	0.1 M KOH	ca. 1.58	N/A	N/A	[74]